The Astrophysical Journal, 849:43 (14pp), 2017 November 1 https://doi.org/10.3847/1538-4357/aa8b62

How Do Stars Gain Their Mass? A JCMT/SCUBA-2 Transient Survey of Protostars in Nearby Star-forming Regions

Gregory J. Herczeg[1], Doug Johnstone[2,3], Steve Mairs[2,3], Jennifer Hatchell[4], Jeong-Eun Lee[5], Geoffrey C. Bower[6], Huei-Ru Vivien Chen[7], Yuri Aikawa[8], Hyunju Yoo[5,9], Sung-Ju Kang[10], Miju Kang[10], Wen-Ping Chen[11], Jonathan P. Williams[12], Jaehan Bae[13], Michael M. Dunham[14,15], Eduard I. Vorobyov[16,17,18], Zhaohuan Zhu[19], Ramprasad Rao[20], Helen Kirk[2], Satoko Takahashi[21,22], Oscar Morata[20], Kevin Lacaille[23], James Lane[3], Andy Pon[24], Aleks Scholz[25], Manash R. Samal[11], Graham S. Bell[26], Sarah Graves[26], E'lisa M. Lee[26], Harriet Parsons[26], Yuxin He[27], Jianjun Zhou[27], Mi-Ryang Kim[28], Scott Chapman[23], Emily Drabek-Maunder[29], Eun Jung Chung[10], Stewart P. S. Eyres[30], Jan Forbrich [15,31], Lynne A. Hillenbrand[32], Shu-ichiro Inutsuka[33], Gwanjeong Kim[10], Kyoung Hee Kim[34], Yi-Jehng Kuan[20,35], Woojin Kwon[10,36], Shih-Ping Lai[7,20], Bhavana Lalchand[11], Chang Won Lee[10,36], Chin-Fei Lee[20], Feng Long[1,37], A-Ran Lyo[10], Lei Qian[38], Peter Scicluna[20], Archana Soam[10], Dimitris Stamatellos[30], Shigehisa Takakuwa[39], Ya-Wen Tang[20], Hongchi Wang[40], and Yiren Wang[1,37]

[1] Kavli Institute for Astronomy and Astrophysics, Peking University, Yiheyuan 5, Haidian Qu, 100871 Beijing, China
[2] NRC Herzberg Astronomy and Astrophysics, 5071 West Saanich Road, Victoria, BC, V9E 2E7, Canada
[3] Department of Physics and Astronomy, University of Victoria, Victoria, BC, V8P 5C2, Canada
[4] Physics and Astronomy, University of Exeter, Stocker Road, Exeter EX4 4QL, UK
[5] School of Space Research, Kyung Hee University, 1732, Deogyeong-Daero, Giheung-gu Yongin-shi, Gyunggi-do 17104, Korea
[6] Academia Sinica Institute of Astronomy and Astrophysics, 645 N. A'ohoku Place, Hilo, HI 96720, USA
[7] Department of Physics and Institute of Astronomy, National Tsing Hua University, Taiwan
[8] Department of Astronomy, University of Tokyo, Tokyo, Japan
[9] Chungnam National University, Korea
[10] Korea Astronomy and Space Science Institute, 776 Daedeokdae-ro, Yuseong-gu, Daejeon 34055, Korea
[11] Graduate Institute of Astronomy, National Central University, 300 Jhongda Road, Zhongli, Taoyuan, Taiwan
[12] Institute for Astronomy, University of Hawaii at Manoa, Honolulu, HI 96822, USA
[13] Department of Astronomy, University of Michigan, 1085 S. University Avenue, Ann Arbor, MI 48109, USA
[14] Department of Physics, The State University of New York at Fredonia, Fredonia, NY 14063, USA
[15] Harvard-Smithsonian Center for Astrophysics, 60 Garden Street, Cambridge, MA 02138, USA
[16] Institute of Fluid Mechanics and Heat Transfer, TU Wien, Vienna, A-1060, Austria
[17] Research Institute of Physics, Southern Federal University, Stachki Ave. 194, Rostov-on-Don, 344090, Russia
[18] University of Vienna, Department of Astrophysics, Vienna, A-1180, Austria
[19] Physics and Astronomy Department, University of Nevada, Las Vegas, USA
[20] Academia Sinica Institute of Astronomy and Astrophysics, P. O. Box 23-141, Taipei 10617, Taiwan
[21] Joint ALMA Observatory, Alonso de Córdova 3107, Vitacura, Santiago, Chile
[22] National Astronomical Observatory of Japan, 2-21-1 Osawa, Mitaka, Tokyo 181-8588, Japan
[23] Department of Physics and Atmospheric Science, Dalhousie University, Halifax, NS, B3H 4R2, Canada
[24] Department of Physics and Astronomy, The University of Western Ontario, 1151 Richmond Street, London, N6A 3K7, Canada
[25] SUPA, School of Physics & Astronomy, North Haugh, St. Andrews, KY16 9SS, UK
[26] East Asian Observatory, 660 N. A'ohōkū Place, Hilo, HI 96720, USA
[27] Xinjiang Astronomical Observatory, Chinese Academy of Sciences, Urumqi, China
[28] Department of Physics, Institute for Astrophysics, Chungbuk National University, Korea
[29] Cardiff University, School of Physics and Astronomy, The Parade, Cardiff, CF24 3AA, UK
[30] Jeremiah Horrocks Institute for Mathematics, Physics & Astronomy, University of Central Lancashire, Preston, PR1 2HE, UK
[31] Centre for Astrophysics Research, School of Physics, Astronomy and Mathematics, University of Hertfordshire, College Lane, Hatfield AL10 9AB, UK
[32] Department of Astronomy; MC 249-17, California Institute of Technology, Pasadena, CA 91125, USA
[33] Department of Physics, Graduate School of Science, Nagoya University, 464-8602, Nagoya, Japan
[34] Korea National University of Education, Taeseongtabyeon-ro, Grangnae-myeon, Heungdeok-gu, Cheongju-si, Chungbuk 28173, Korea
[35] Department of Earth Sciences, National Taiwan Normal University, Taipei 116, Taiwan
[36] Korea University of Science and Technology, 217 Gajang-ro, Yuseong-gu, Daejeon 34113, Korea
[37] Department of Astronomy, Peking University, Yiheyuan 5, Haidian Qu, 100871 Beijing, China
[38] National Astronomical Observatories, Chinese Academy of Sciences, Beijing, China
[39] Department of Physics and Astronomy, Graduate School of Science and Engineering, Kagoshima University, 1-21-35 Korimoto, Kagoshima, Kagoshima 890-0065, Japan
[40] Purple Mountain Observatory, & Key Laboratory for Radio Astronomy, Chinese Academy of Sciences, 2 West Beijing Road, Nanjing 210008, China
Received 2017 June 9; revised 2017 September 5; accepted 2017 September 6; published 2017 October 27

Abstract

Most protostars have luminosities that are fainter than expected from steady accretion over the protostellar lifetime. The solution to this problem may lie in episodic mass accretion—prolonged periods of very low accretion punctuated by short bursts of rapid accretion. However, the timescale and amplitude for variability at the protostellar phase is almost entirely unconstrained. In A James Clerk Maxwell Telescope/SCUBA-2 Transient Survey of Protostars in Nearby Star-forming Regions, we are monitoring monthly with SCUBA-2 the submillimeter emission in eight fields within nearby (<500 pc) star-forming regions to measure the accretion variability of protostars. The total survey area of ~1.6 deg^2 includes ~105 peaks with peaks brighter than 0.5 Jy/beam (43 associated with embedded protostars or disks) and 237 peaks of 0.125–0.5 Jy/beam (50 with embedded protostars or disks). Each field has enough bright peaks for flux calibration relative to other peaks in the same field,

which improves upon the nominal flux calibration uncertainties of submillimeter observations to reach a precision of ∼2%–3% rms, and also provides quantified confidence in any measured variability. The timescales and amplitudes of any submillimeter variation will then be converted into variations in accretion rate and subsequently used to infer the physical causes of the variability. This survey is the first dedicated survey for submillimeter variability and complements other transient surveys at optical and near-IR wavelengths, which are not sensitive to accretion variability of deeply embedded protostars.

Key words: stars: formation – stars: protostars – stars: variables: T Tauri, Herbig Ae/Be – submillimeter: stars

1. Introduction

Low-mass stars form through the gravitational collapse of molecular cloud cores. The evolution of mass accretion onto a forming protostar depends on the rate at which the interior of the core collapses, the role of the circumstellar disk as a temporary mass reservoir and transportation mechanism, and the physics of how the inner disk accretes onto the stellar surface. In dynamical models of gravitational collapse of a spherical protostellar core (e.g., Shu 1977; Shu et al. 1987; Masunaga & Inutsuka 2000), the young star grows steadily from the infalling envelope at a rate of a few $10^{-6}\,M_{\odot}\,\mathrm{yr}^{-1}$. However, Kenyon et al. (1990) found that luminosities of most protostars fall far below those expected from energy release by steady accretion over protostellar lifetimes. This luminosity problem has since been confirmed with an improved census of protostars (e.g., Enoch et al. 2009; Dunham et al. 2010; see also discussions in Dunham et al. 2014 and Fischer et al. 2017).

The resolution of the luminosity problem likely requires either a time-dependent or mass-dependent accretion rate (e.g., discussions in Hartmann et al. 2016 and Fischer et al. 2017; see also, e.g., Offner & McKee 2011; Myers 2012). Observationally, strong but mostly indirect evidence suggests that the accretion rate is punctuated by short bursts of rapid accretion, often termed *episodic accretion* (Kenyon et al. 1990; Dunham et al. 2010; Dunham & Vorobyov 2012). The form of this time dependence may have a lasting affect on the evolution of stars (e.g., Hartmann et al. 1997; Baraffe & Chabrier 2010; Baraffe et al. 2017; Vorobyov et al. 2017a), the physical structure of disks and their propensity to fragment (e.g., Stamatellos et al. 2011, 2012; Vorobyov et al. 2014), and the chemistry of disks and envelopes (e.g., Kim et al. 2012; Jørgensen et al. 2013; Vorobyov et al. 2013; Visser et al. 2015; Harsono et al. 2015; Owen & Jacquet 2015; Cieza et al. 2016).

The suggestion of accretion bursts in protostars has significant support from later stages of pre-main-sequence stellar evolution. Spectacular outbursts[41] with optical brightness increases of ∼5 mag are interpreted as accretion rate increases of two orders of magnitude and can last for months (called EXors following the prototype EX Lup, e.g., Herbig 2008; Aspin et al. 2010) or decades (called FUors following the prototype FU Ori, e.g., Herbig 1977; Hartmann & Kenyon 1996). Because most transient searches use optical photometry, these accretion outbursts are detected only on young stellar objects that are optically bright and are therefore biased to variability at or near the end of their main phase of stellar growth. Only a few outbursts have been detected on a deeply embedded Class 0 star (Kóspál et al. 2007; Safron et al. 2015; Hunter et al. 2017), the stage when the star should accrete much of its mass—although many FUor objects retain some envelopes and are classified as Class I objects (e.g., Zhu et al. 2008; Caratti o Garatti et al. 2011, Caratti O Garatti et al. 2016; Fischer et al. 2012; Green et al. 2013; Kóspál et al. 2017). Indirect evidence for outbursts includes chemical signatures of past epochs with high luminosity (e.g., Kim et al. 2012; Vorobyov et al. 2013; Jørgensen et al. 2015; Frimann et al. 2017) and periodic shocks/bullets along protostellar jets, which may offer a historical record of accretion events (e.g., Reipurth 1989; Raga et al. 2002; Plunkett et al. 2015). In addition to these large events, instabilities in the inner disk likely lead to more frequent but smaller bursts of accretion, as seen in more evolved disks (e.g., Costigan et al. 2014; Venuti et al. 2014; Cody et al. 2017).

Directly observing either large outbursts or accretion flickers on protostars is challenging because they are deeply embedded in dense envelopes. The accretion luminosity is not directly visible to us, and is instead absorbed by the envelope and reprocessed into photons with lower energies, which then escape from the system. Models of an accretion burst indicate that the enhanced accretion luminosity heats dust in the envelope (Johnstone et al. 2013). The dust is then seen as brighter emission at far-IR through submillimeter wavelengths. The change in luminosity is strongest at far-IR wavelengths, which traces the effective photosphere of the envelope, where the envelope becomes transparent when the local temperature drops below ∼100 K. Single-dish observations at submillimeter wavelengths have large scales, which tends to probe the temperature structure of the outer envelope. When the protostellar luminosity increases, the outer envelope is expected to become hotter. Since the atmosphere of the Earth is opaque in the far-IR, and the most heavily embedded objects are not visible at optical/near-IR wavelengths, submillimeter observations provide us with our best ground-based window into the protostar—a snapshot of the accretion rate, averaged over the timescale of a few weeks for the luminosity burst to propagate through the envelope. While some far-IR/submillimeter variability has indeed been detected on protostars, these detections are mostly based on transients identified in optical/near-IR surveys and have few epochs of flux measurements at far-IR/submillimeter wavelengths (e.g., Billot et al. 2012; Scholz et al. 2013a; Balog et al. 2014; Onozato et al. 2015; Safron et al. 2015).

In this paper, we describe our novel James Clerk Maxwell Telescope (JCMT) survey, A JCMT/SCUBA-2 Transient Survey of Protostars in Nearby Star-forming Regions, shortened to *JCMT-Transient*, in which we use Submillimetre Common-User Bolometer Array 2 (SCUBA-2; Holland et al. 2013) to monitor the submillimeter flux of deeply embedded protostars in eight fields within nearby star-forming regions. This is the first dedicated long-term submillimeter monitoring program. The only previous submillimeter monitoring programs probed variability in synchrotron radiation from the Sagittarius A* at the galactic center over five consecutive nights (Haubois et al. 2012) and the black hole

[41] The classification scheme of EXor and FUor outbursts is sometimes vague, with both classes likely including diverse phenomenon.

Table 1
Description of the Eight Selected Fields

Name	Location	Dist.	# of Peaks[a]				*Spitzer* Sources[b]			Class 0/I[c]		Disks[c]	
		pc	>0.125	>0.25	>0.5	>1.0	0/I	Flat	II	>0.125	>0.5	>0.125	>0.5
Perseus—NGC 1333	032854+311652	270[d]	33	24	10	6	34	14	62	14	6	1	0
Perseus—IC348	034418+320459	303[d]	12	4	3	2	13	8	114	5	3	0	0
Orion A—OMC2/3	053531−050038	388[e]	120	77	41	25	64	⋯	600	12	10	12	4
Orion B—NGC 2024	054141–015351	423[e]	38	14	8	4	26	⋯	232	3	2	1	0
Orion B—NGC 2068	054613–000605	388[e]	31	24	12	5	22	⋯	117	9	6	0	0
Ophiuchus	162705–243237	137[f]	41	23	7	3	21	30	87	12	1	6	2
Serpens Main	182949+011520	436[g]	16	15	10	7	19	9	51	8	7	0	0
Serpens South	183002–020248	436[g]	51	27	14	2	50	34	142	10	1	1	0

Notes.
[a] Number of individual peaks with SCUBA-2 850 μm flux brighter than listed.
[b] Total number of protostars in the field, as identified by Stutz et al. (2013), Dunham et al. (2015), and Megeath et al. (2016).
[c] Protostars and disks located within 7″ of a peak, see also the Appendix.
[d] This work using parallaxes from the *Gaia* DR1 TGAS catalog.
[e] Parallaxes from the VLBI GOBELINS program (Kounkel et al. 2017).
[f] Parallax from the VLBI GOBELINS program (Ortiz-León et al. 2017b).
[g] Parallaxes from the VLBI GOBELINS program (Ortiz-León et al. 2017a).

X-ray binary V404 Cyg over 4.5 hr (Tetarenko et al. 2017). Although large outbursts, with a factor of 100 increases in source luminosity, are rare (Scholz et al. 2013a; Hillenbrand & Findeisen 2015), our survey should also reveal the lower-amplitude variability (with changes of a factor of <10 in luminosity) that are commonly detected on classical T Tauri stars. In Section 2, we describe our observational plans. In Section 3, we describe initial results, including the stability of our flux calibration. In Section 4, we discuss the expected contributions of this survey to our understanding of protostellar variability and related applications for this data set. In Section 5, we discuss ancillary science related to disks, VeLLOs, filaments, and nonthermal emission. In Section 6, we discuss our expectations for the future results from this program.

2. Overview of Survey Methodology

Our ongoing JCMT survey program, M16AL001, consists of monitoring 450 and 850 μm emission from eight young regions that are rich in protostars, as identified in previous Spitzer, Herschel, and SCUBA-2 Gould Belt Surveys. Submillimeter monitoring surveys have been challenging in the past because of calibration uncertainties. The wide SCUBA-2 field of view allows us to use multiple bright sources in the same field to calibrate the image relative to other bright objects in the field, the submillimeter equivalent of differential photometry.

2.1. Sample Selection

We selected eight 30′ regions of nearby (<500 pc), active star formation to maximize the number of protostars and disks in the fields, with a preference to the youngest regions while also avoiding regions with the most complex, confused features. The fields include a total of 182 Class 0/I objects, 132 flat-spectrum objects, and 670 disks (see Table 1), as previously classified from *Spitzer* SEDs by Dunham et al. (2010), Stutz et al. (2013), and Megeath et al. (2016). Each region includes 3–41 peaks with 850 μm fluxes above 0.5 Jy/beam and 12–120 peaks above 0.12 Jy/beam, and 3–14 protostars associated with those peaks. All requested fields have a past epoch from the JCMT Gould Belt Survey (Ward-Thompson et al. 2007), along with complementary *Spitzer* mid-IR (Dunham et al. 2015; Megeath et al. 2016) and Herschel far-IR imaging (André et al. 2014).

2.2. Observing Strategy

The SCUBA-2 instrument is a 10,000 pixel bolometer camera that images simultaneously at 450 and 850 μm with 9.″8 and 14.″6 resolution (Dempsey et al. 2013; Holland et al. 2013). Both focal planes consist of four subarrays of 1280 bolometers that simultaneously cover a field with an ∼8′ diameter. The regions are observed in a pong 1800″ pattern, in which SCUBA-2 scans over a field of view of 30′ diameter to produce an image with smooth sensitivity across the map (Kackley et al. 2010).

Our observations are being obtained in weather bands 1–3, which correspond to different levels of atmospheric H_2O column densities that lead to opacities of $\tau < 0.12$ at 225 GHz. Mairs et al. (2017a) provide a complete list of observations obtained through 2017 February, including τ and sensitivity. To date, 21% of our observations have been obtained in Band 1 (the driest weather, $\tau < 0.05$ at 225 GHz) and 39% have been observed in Band 2 ($0.05 < \tau < 0.08$). The exposure time for each individual epoch is 20–40 min., adjusted for the atmospheric opacity to achieve a sensitivity of 12 mJy/beam per 3″ square pixel at 850 μm.[42] Each field is being observed once per month when available, with the first observations obtained in 2015 December and an initial program that runs through 2019 January. Since JCMT operations can extend a few hours into dawn, each field will be observed ∼10 times per year. When all images are stacked, the total sensitivity at 850 μm will be ∼2.5 mJy/beam (compared to ∼4 mJy/beam for the Gould Belt Survey, Mairs et al. 2015).

This monthly cadence is selected based on estimates of how quickly a luminosity burst would propagate through the envelope and be detectable, following the radiative transfer and envelope models calculated by Johnstone et al. (2013). Because submillimeter photons from an envelope are emitted

[42] This paper quotes sensitivities as pixel-to-pixel variation derived using a beam size of 14.6 arcsec and a pixel size of 3 arcsec, which is consistent with the sensitivities in Mairs et al. (2017a) but may differ from methodologies in other studies.

from a large volume, the light propagation time is a few weeks. Once irradiated, the dust heating timescale is negligible because dust has a low heat capacity. Therefore, a 1 month cadence is selected as the estimated optimal cadence for sensitivity to accretion variability on weeks-to-months timescales. This cadence will also allow us to stack several images over a few months to characterize any smooth long-term changes in the flux and to evaluate variability of fainter objects in our field. This stacking will reduce the flux calibration uncertainties introduced stochastically by changes of the optical depth of the atmosphere on timescales shorter than the integration time.

2.3. Data Reduction and Source Extraction

A full description of the data reduction and flux calibration is provided in the companion paper by Mairs et al. (2017a), following on the methods developed by Mairs et al. (2015) and filtering on scales of 200″. Compact peaks are measured using the JCMT Science Archive algorithm JSA_catalog (see the PICARD package in Starlink, Gibb et al. 2013, and the Appendix). These peaks are not fully vetted. Appendix A includes only those peaks that are established to be associated with a nearby disk or protostar, with a submillimeter centroid located <7″ from the centroid of the mid-IR peak (see the Appendix for further details).

Since flux variability will be converted into a change in protostellar accretion luminosity, the accuracy of our flux calibration determines our sensitivity to accretion events. Standard flux calibration for submillimeter imaging with SCUBA-2 (and other similar instruments) is calculated from contemporaneous observations of flux standards and simultaneous measurements of the atmospheric opacity. This standard approach to flux calibration is accurate to ∼7%–10% (Dempsey et al. 2013).

To improve upon this standard approach, we leverage the presence of many protostars within single submillimeter fields to improve the accuracy of our fluxes by calibrating the fluxes relative to other sources in the same image. A set of stable, bright peaks is identified within each field and then used to provide the relative calibration for each image, achieving a flux accuracy of ∼2%–3% (Mairs et al. 2017a). This quantified uncertainty also establishes the confidence level that any detected variability is attributed to the source, rather than possible contributions because of changes in atmospheric transmission. For faint targets, images will be stacked to look for variability on longer timescales.

Our science results to date focus on 850 μm images. Imaging at 450 μm is sensitive to objects in our field only during observations obtained with low precipitable water vapor (Band 1 or Band 2 weather, about 60% of epochs). Since our techniques for quantifying variability require many epochs per field, analyses of 450 μm images will occur after we have obtained enough imaging in the best weather bands and developed techniques for the analysis of 850 μm images.

3. Description of Fields and Sources

The eight star-forming regions in this survey (Figure 1) were chosen as follows. We analyzed the JCMT Legacy Release Peak Catalog of observed 850 μm submillimeter peaks (S. Graves et al., in preparation) to find 30″-wide fields with the largest number of submillimeter sources, using these as a proxy for star-formation activity. Typically, the brightest (most massive) submillimeter peaks in star-forming regions are found to be associated with deeply embedded protostars (e.g., Jørgensen et al. 2007, 2008) and are interpreted as the molecular core out of which the star is forming. A subset of these bright (massive) peaks are not known to harbor protostars and are interpreted as being at an earlier evolutionary stage, i.e., starless or prestellar (see, e.g., Sadavoy et al. 2010 and Pattle et al. 2015, 2017). As the submillimeter peaks get fainter (lower envelope mass), the association with protostars diminishes, although the mass function of the starless cores subset suggests that they may still be related to the star-formation process (e.g., Motte et al. 1998). Many of the fainter peaks may be wispy structures within the molecular cloud and not directly related to ongoing star formation. Some fainter emission peaks may be disks associated with Class II protostars.

Figure 2 and Table 1 show the total number of sources with peak 850 μm flux brighter than 0.125 Jy/beam for all regions in our survey, sorted by brightness bin and by association with protostars and disks (see also the Appendix). To better understand the distribution of protostellar cores versus starless cores in our regions, we collated the submillimeter peaks against catalogs of known protostars (Class 0/I objects) and disks (Class II objects), as identified in past *Spitzer* photometry (Dunham et al. 2015; Megeath et al. 2016) as well as extensive submillimeter imaging (e.g., Johnstone & Bally 1999; Hatchell et al. 2005; Enoch et al. 2006, 2007; Johnstone et al. 2006; Kirk et al. 2006). Of the 342 bright peaks, 73 are associated with known protostars (Class 0/I) and 20 are associated with known disks (Class II). Given the poor resolution of the JCMT, some of these associations may be coincidental, particularly in the case of disks (most of which are too faint to be detected with our sensitivity). Moreover, since the determination of protostellar class is often ambiguous, some sources identified as disks are more deeply embedded sources, if for example the source is viewed through a hole in the envelope. Similarly, some of the most deeply embedded protostars are missed by the surveys due to extreme extinction, even in the mid-IR, so the lack of association of a peak with a known protostar does not rule out the presence of a protostar within the peak. Indeed, Stutz et al. (2013) found a few PACS Bright Red Sources (PBRs) objects at 70 μm with Hershel that were entirely unseen with Spitzer. Given these caveats, the numbers presented here should provide a reasonable measure of the degree of star-formation activity taking place in the observed peaks in our survey, but any variability that we uncover will require more careful consideration of the individual peak and any neighboring protostar.

The following subsections describe each region in more detail.

3.1. NGC 1333—Perseus

NGC 1333 is in many ways a prototypical nearby star-forming cluster, with a mass of 450 $M_\odot$ and with a diameter of ∼1–2 pc, located within the large-scale Perseus star-forming complex (e.g., Bally et al. 2008; Walawender et al. 2008). The temperatures of the regions in NGC 1333 range from 10–14 K for filaments and ambient cloud material, are ∼20 K on the southern edge of the cloud, and reach 40 K near the B star SVS3 and the embedded protostar IRS 6 (Hatchell et al. 2013; Chen et al. 2016). The distance estimated from the *Gaia* TGAS catalog (Gaia Collaboration et al. 2016)[43] of 271 ± 20 pc is

[43] The *Gaia* TGAS DR1 catalog contains two likely members within 15′ of the cluster center with distances of 274^{+18}_{-20} pc and 267^{+19}_{-21} pc (Gaia Collaboration et al. 2016).

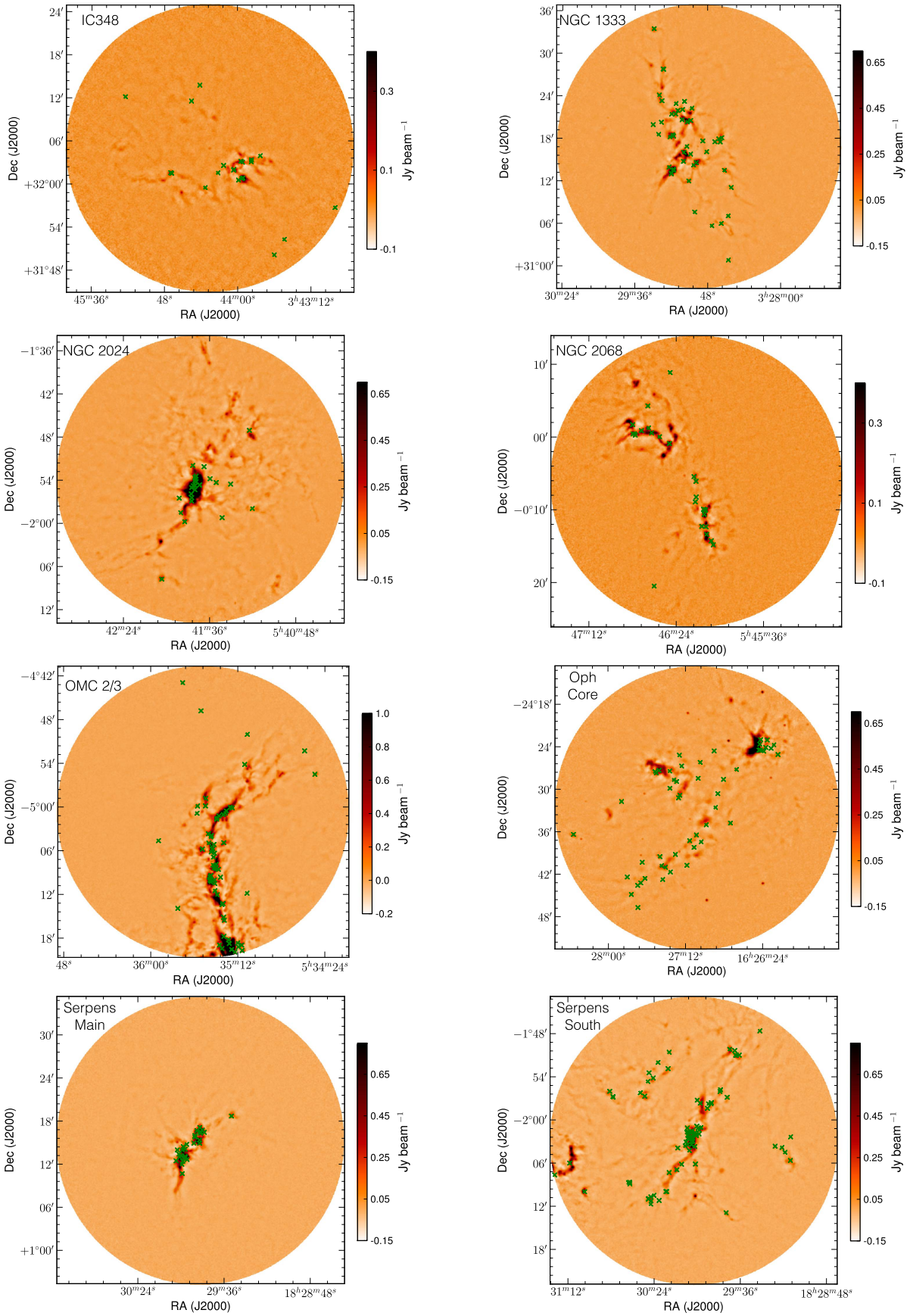

Figure 1. SCUBA-2 850 μm images of all eight regions in our survey, co-added over the first year of data (see also Mairs et al. 2017a). The marks show the location of Class 0, Class I, and flat spectrum protostars, as identified and classified by Dunham et al. (2015) and Megeath et al. (2016).

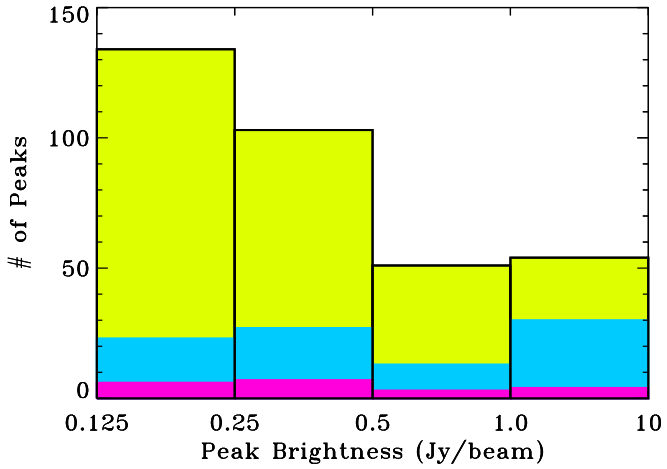

Figure 2. Distribution of 342 peaks with 850 μm peak brightness above 0.125 Jy/beam for all eight regions in our survey (yellow). The purple and blue histograms, respectively, show the number of peaks associated with one or more disks and protostars. Based on the analysis of Mairs et al. (2017a), we can achieve 2%–3% accuracy for the 105 peaks brighter than 0.5 Jy/beam and 10% for the 237 sources with brightness 0.125–0.5 Jy/beam. Of these 342 peaks, 93 are associated with distinct protostars or disks. In some cases, multiple protostars are blended together to form a single peak at the resolution of JCMT.

consistent with previous distance estimates of 220–320 pc (see the discussion in Scholz et al. 2013b) and would imply that NGC 1333 is located in the foreground of the Perseus star-forming cloud.

Members range from two massive B-stars down to objects with estimated masses of a few Jupiter masses, with a distribution consistent with a single power law from low-mass stars to brown dwarfs (Scholz et al. 2012a, 2012b; Rebull et al. 2014; Luhman et al. 2016). Gutermuth et al. (2008a) found that ~30% of stars with a mid-IR excess are embedded Class I protostars, which when combined with a lack of a strong central condensation and localized extinction together point to an early evolutionary state for the cloud. The commonly adopted age of 1–2 Myr for NGC 1333 is slightly younger than that of IC 348, although isochrone fits to optical/near-IR members do not show a significant age difference between the two clusters (Luhman et al. 2016). NGC 1333 also harbors several dozen Herbig–Haro objects (e.g., Bally et al. 1996; Yan et al. 1998) with associated molecular line emission (Knee & Sandell 2000; Curtis et al. 2010).

3.2. IC 348—Perseus

IC 348 is a nearby star cluster associated with the Perseus cloud complex and is located at ~303 pc, as measured from parallax measurements.[44] With an average age of 3–5 Myr (e.g., Luhman et al. 2016), IC 348 is older than the other regions in this survey and was selected because of the high density of protostellar disks within the field of view, along with a few protostars. Thirteen disks were detected in previous deep SCUBA-2 images of 850 μm emission (Cieza et al. 2015). Southwest of the main cluster is a protostellar cluster, with dense molecular clouds, Class 0/I protostars and Herbig–Haro objects (e.g., Walawender et al. 2006).

3.3. OMC-2/3—Orion

The Orion Molecular Cloud 2/3 region (OMC-2/3) is located in the northern part of the Orion Molecular Cloud (OMC, Bally et al. 1987; Mezger et al. 1990) and is often referred to as the integral-shaped filament (Johnstone & Bally 1999; Salji et al. 2015; Lane et al. 2016). Our pointing includes the northern half of the integral-shaped filament and contributes roughly 40% of the total number of bright peaks in our survey. The OMC 2/3 region, located at $d = 388$ pc from the GOBELINS VLBI parallax survey (Kounkel et al. 2017), is one of the best-studied and richest nearby star-forming regions at all observable wavelengths (e.g., Johnstone & Bally 1999; Tsujimoto et al. 2002; Megeath et al. 2012) and has a disk/envelope fraction of 20% (e.g., Chini et al. 1997; Nutter & Ward-Thompson 2007; Peterson et al. 2008; Megeath et al. 2012; Takahashi et al. 2013). Two sources in this region are deeply embedded PACS Bright Red Sources (PBRs) identified using far-IR photometry (Stutz et al. 2013; Tobin et al. 2015). This region also includes (arguably) the first detected outburst of a Class 0 protostar (Safron et al. 2015). Most protostars are located along the densest part of the molecular filaments, while Class II sources are distributed over the region. Submillimeter CO emission line surveys have revealed ~15 molecular outflows within this region (Aso et al. 2000; Williams et al. 2003; Takahashi et al. 2008, 2012).

3.4. NGC 2024—Orion

NGC 2024 (the Flame Nebula) is located within the Orion B (L1630) cloud complex, one of the nearest active high-mass star-forming regions (see the review by Meyer et al. 2008), located at a distance of ~388 pc (Kounkel et al. 2017). The region is one of the densest of all clouds in Orion, with a protostellar density of ~50 pc^{-2} (Skinner et al. 2003; Megeath et al. 2016) spread over a virial radius of 0.4 pc (Lada et al. 1997). A long molecular ridge corresponds to the regions of highest extinction and includes many dense cores (e.g., Thronson et al. 1984; Visser et al. 1998; Choi et al. 2012). Within the molecular ridge, two clumps of protostars are especially bright in sub-mm dust continuum emission, revealing a total mass of 633 $M_\odot$ (Johnstone et al. 2006; Kirk et al. 2016).

3.5. NGC 2068 and HH 24—Orion

NGC 2068 and HH24 (together referred to as NGC 2068 throughout this paper) are also located within the Orion B cloud complex, with HH 24 to the south of NGC 2068 (Kutner et al. 1977; Bontemps et al. 1995; Gibb 2008). The census of near-IR and mid-IR protostars leads to total masses of NGC 2068 and HH 24 of ~240 $M_\odot$ and 120 $M_\odot$, respectively (Spezzi et al. 2015). The protostellar population includes several PBRs (e.g., Stutz et al. 2013) and the eruptive protostar V1647 Ori (also known as McNeil's nebula; Reipurth & Aspin 2004).

[44] Five members of IC348 are in the *Gaia* DR1 TGAS catalog (Gaia Collaboration et al. 2016), with an average parallax distance of 303 ± 21 pc, where the uncertainty is dominated by the systematic error of ~0.3 mas. This distance is consistent with past measurements from *Hipparcos* (van Leeuwen 2007) and other methods (see the discussion in Herbst 2008).

3.6. Ophiuchus Core

The Ophiuchus molecular cloud spans 30 pc^2 on the plane of the sky and contains over 3000 solar masses of gas (e.g., Wilking et al. 2008; Dunham et al. 2015). Star formation in the Ophiuchus complex may have been triggered by the Sco-Cen OB association, and includes numerous streamers of molecular gas pointing away from Sco-Cen (e.g., Vrba 1977; Loren & Wootten 1986; Wilking et al. 2008). The parallax distance adopted here of 137 pc from the GOBELINS survey (Ortiz-León et al. 2017a) is slightly larger than previous distance measurements of ∼120 pc to the cluster (Loinard et al. 2008).

The most active portion of the Ophiuchus cloud complex is L1688, which stands out from other nearby low-mass star-forming regions because the star-forming environment is more clustered (Motte et al. 1998; Johnstone et al. 2000; Allen et al. 2002; Johnstone et al. 2004; Stanke et al. 2006; Young et al. 2006). L1688 shows significant substructure, with 13 identified peaks, many of which contain multiple starless and protostellar cores (Loren et al. 1990; Motte et al. 1998; Kamazaki et al. 2001; Johnstone et al. 2004; Stanke et al. 2006; Young et al. 2006; Nakamura et al. 2012; White et al. 2015; Pan et al. 2017). The Oph A clump, in the northwest corner of L1688, has the highest column densities and temperatures (Motte et al. 1998; Johnstone et al. 2000; Friesen et al. 2009; Pon et al. 2009; Pan et al. 2017), and appears as a bright crescent of continuum emission wrapping around the position of the nearby B star S1 (Elias 1978). The prototype for the class 0 protostellar stage, VLA 1623 (André et al. 1993), is located within this field.

3.7. Serpens Main

The Serpens Main region is an active star-forming region (Strom et al. 1976; Eiroa et al. 2008) with a total mass of 230–300 $M_\odot$ (Olmi & Testi 2002; Graves et al. 2010) located at 436 ± 9 pc (from the GOBELINS survey Ortiz-León et al. 2017a). The SE and NW substructures are bright in submillimeter/millimeter dust continuum emission (Casali et al. 1993; Davis et al. 1999; Kaas et al. 2004). The protostars and ongoing star formation in Serpens Main is highly concentrated at the center of our pointing. The sources in early evolutionary stages (Class 0/I and Flat SEDs) are clustered in small regions while the older Class II and III sources are distributed outside of these clusters (Harvey et al. 2007).

The velocity field of Serpens Main shows the presence of global infall motion, outflow, rotation, and turbulence (Olmi & Testi 2002). The velocity field in the NW subcluster is relatively uniform, on the other hand, while the SE subcluster has a more complicated velocity structure showing a large velocity dispersion (>0.5 km s^{-1}) at the central region (Duarte-Cabral et al. 2010; Graves et al. 2010; Lee et al. 2014). The NW subcluster includes known IR-variables OO Ser, EC 53, and EC 37 (Hodapp 1999; Kóspál et al. 2007; Hodapp et al. 2012). Submillimeter variability of the protostar EC 53, which was uncovered in this survey, will be presented in Yoo et al. (2017).

3.8. Serpens South

Serpens South is an active star-forming region within the Aquila Rift molecular complex, located at 436 ± 9 pc (Ortiz-León et al. 2017a) and ∼3° south of Serpens Main (Kern et al. 2016). Gas is flowing inward onto the filaments to supply the fuel for star formation (Kirk et al. 2013). Maury et al. (2011) measure a total mass of the cluster of ∼1660 $M_\odot$, adjusted for the updated distance (see Friesen et al. 2016). The ratio of Class 0/Class I sources of ∼77% and the Class I to Class II ratio of about 80% are among the highest fractions for nearby star-forming regions (Gutermuth et al. 2008b; Maury et al. 2011).

4. Testing Models of Protostellar Accretion

During protostellar accretion, viscous processes in the disk transport angular momentum outward, allowing gas to flow inward toward the protostar. The source of viscosity in protostellar disks is uncertain (e.g., Armitage 2015; Hartmann et al. 2016); it could be due to turbulence or instabilities (gravitational, magnetorotational) that develop where the conditions are right. When the accretion rate through some radius in the disk is lower than the accretion rate at larger radii, material builds up until the accretion rate through the inner disk adjusts. A steady accretion flow through the disk and onto the star is determined by the most stringent bottleneck, with short periods of strong accretion when that bottleneck breaks. Both the amplitude of the nonsteady accretion and the timescale over which the accretion varies are likely to span a wide range of values. Models of these accretion processes provide predictions for the frequency and amplitude of accretion variability, with limitations related to physical scales and MHD microphysics.

Prospects for detecting accretion variability depend on the size and location of instabilities within the disk. In the past, outbursts on young stars have been differentiated into EXors and FUors based on timescales and spectral characteristics, although it remains unclear whether these events have different physical causes or are simply different manifestations of similar phenomena (e.g., Audard et al. 2014). Several mechanisms have been proposed to explain short- and long-term variability, including gravitational instabilities in the outer disk region (Vorobyov & Basu 2005, 2015; Machida et al. 2011), thermal instabilities in the inner disk region (Hartmann & Kenyon 1985; Lin et al. 1985; Bell et al. 1995), a combination of gravitational instabilities in the outer disk region and the magnetorotational instability in the inner disk region (Armitage et al. 2001; Zhu et al. 2009, 2010), spiral-wave instabilities (Bae et al. 2016; Hennebelle et al. 2017), gravitational interactions with companions or passing stars (Bonnell & Bastien 1992; Forgan & Rice 2010; Green et al. 2016; Muñoz & Lai 2016), and magnetospheric instabilities (e.g., D'Angelo & Spruit 2010; Romanova et al. 2013; Armitage 2016). Some of these processes lead to the rare accretion bursts of FUors and the much more common variation of accretion seen on classical T Tauri stars (e.g., Costigan et al. 2014; Venuti et al. 2014; Cody et al. 2017), while others may cause periodic accretion bursts, as seen in a few objects (Hodapp et al. 2012; Muzerolle et al. 2013; Hodapp & Chini 2015).

While only some of these theoretical ideas are capable of providing significant mass accretion variability over the lifetime of embedded protostars, all should produce observable signatures in accretion luminosity with characteristic amplitudes and timescales. Assuming that accretion is related to disk transport processes on orbital timescales, the variability will

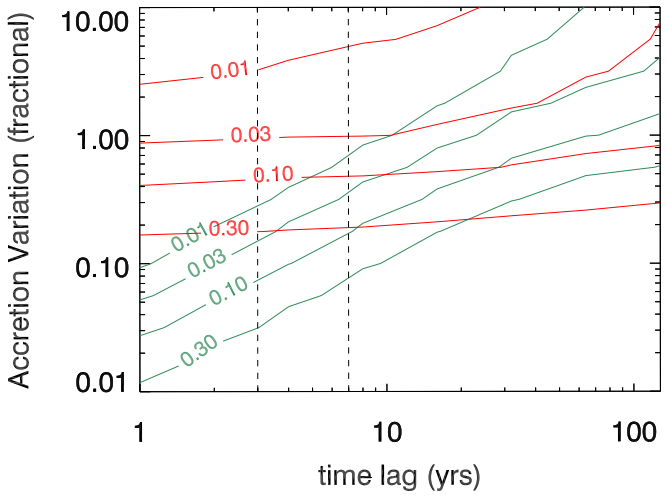

Figure 3. Expected fraction of time that a given theoretical model returns an amplitude variation greater than a specific amount as a function of the time lag between observations. The green contours show results for a Vorobyov & Basu (2010) model in which accretion variability is driven by large-scale modes within the gravitationally unstable disk. The red contours show the result for a Bae et al. (2014) model in which accretion variability is driven by the activation of the magnetorotational instability in the otherwise magnetically inert inner disk, via heating from gravitational instability-driven spiral waves. The contours are labeled with the fraction of stars that would show the level of variability. In both models, larger amplitudes correlate with longer times. The dashed lines denote a three-year separation in time for our survey and a seven-year separation in time between earlier epochs from the JCMT Gould Belt Survey and the end of our survey.

depend on the radii where the physical transport processes originate and will range from days in the inner disk to hundreds of years in the outer disk. Within deeply embedded protostars, the range of accretion events taking place is almost entirely unconstrained from both theoretical and observational perspectives.

Monitoring the brightness of deeply embedded protostars with a flux calibration uncertainty of 2%–3% (Mairs et al. 2017a) will produce direct measurements of both the range of accretion events and their duration, provided that the duration is longer than a few days and that the accretion is radiative and not optically thick. Since the total luminosity change is ∼10 times larger than any change expected from the dust continuum emission at 850 μm (Johnstone et al. 2013), a 3% calibration uncertainty corresponds to a ∼30% uncertainty in the protostar luminosity. The power spectrum of accretion variability on young objects will then provide a diagnostic for the size and location of disk instabilities (Elbakyan et al. 2016), independent of whether the majority of the mass is accreted in rare large events. In addition to these changes from accretion luminosity, single-epoch brightness increases may be detected from any star in our field and attributed to either short accretion bursts or nonthermal synchrotron emission (see Section 5.4).

Our monitoring of 342 peaks brighter than 0.125 mJy/beam (73 of which are associated with protostars and 20 with disks) will then provide an unbiased survey of variability on a large enough data set for robust statistical analyses. The starless cores should not be variable and therefore provide a control sample in statistical analyses. Within our fields, 176 more protostars are fainter than 0.125 mJy/beam but increase the sample size for a search for flux increases of factors of 2–10. While these large bursts are expected to be rare, models of accretion variability suggest that annual variations of 10% may be common. Figure 3 presents this analysis as applied to the outburst models of Bae et al. (2014) and Vorobyov & Basu (2015), with clear differences in the observational signatures of accretion variability on short (less than five-year) timescales that result from the different input physics. In the Bae model, >30% of sources will vary by 10% (our 3σ detection limit) over our 3.5-year program, while in the Vorobyov & Basu model ∼7% of sources would be variable at the 10% level. Vorobyov & Basu (2015) predict that fewer bursts should occur during the Class 0 stage than during the Class I stage.

These values suffer from large uncertainties because neither model was designed to resolve short timescales or the small distances over which the last steps of accretion occur. However, they provide some guidance on how this program could be used as a test of models for disk accretion. Moreover, a nondetection of variability on this sample would indicate that the accretion flow moves smoothly through the inner disk, placing a stringent requirement on the instability physics in the inner disk at young ages.

Our initial investigations will search for short-term variability, as found in EC 53 (Yoo et al. 2017), and will also place limits on the stability of bright objects in our sample over the first year of our program and in comparison to the Gould Belt Survey observations obtained ∼3–4 years ago (Mairs et al. 2017b). Once our survey is completed, we will analyze all 450 and 850 μm imaging from our survey plus the Gould Belt Survey to identify any long-term secular changes during our ∼3 years of monitoring, and with ∼7 year time baselines when including the Gould Belt Survey.

5. Related Science Goals

After our first year of data, the stacked image from each region yields a 1σ noise level of ∼4 mJy/beam at 850 μm, similar to the depth of SCUBA-2 imaging from the JCMT Gould Belt Survey (Mairs et al. 2015) and to the deep SCUBA-2 disk surveys in the σ Ori, λ Ori, and IC 348 star-forming regions (Williams et al. 2013; Ansdell et al. 2015; Cieza et al. 2015). The final stacked image after three years of monitoring should achieve a sensitivity of ∼2.5 mJy/beam. These deep images will be useful for studying very low luminosity protostars, faint filamentary structures, disks, and nonthermal synchrotron emission, as described below.

5.1. Very-low-luminosity Objects (VeLLOs)

VeLLOs are protostars with luminosities $\leqslant 0.1\,L_{\odot}$, first discovered in *Spitzer* observations of cores thought at the time to be starless (e.g., Young et al. 2004; Bourke et al. 2006; Dunham et al. 2008; Hsieh et al. 2015). Their very low luminosities are explained by either low accretion rates or low protostellar masses, if they are proto-brown dwarfs (e.g., Lee et al. 2009, 2013; Hsieh et al. 2016). The class of VeLLOs may even include some first cores, which have short lifetimes of 10^3 years before the protostar is created (Larson 1969; Masunaga & Inutsuka 2000). Using coupled disk hydrodynamics and stellar evolution models, Vorobyov et al. (2017b) demonstrate that the characterization of VeLLOs depends on the energy of the gas accreted onto the central object. VeLLOs

are only expected to occur if some time intervals have very low accretion rates, thereby implying other times have high accretion rates. Our observations will reach a 3σ sensitivity of $\sim 10^{-3}\,M_{\odot}$ in envelope mass (depending on temperature and opacity) for all regions, and should therefore be capable of unambiguously identifying proto-brown dwarfs in our target fields. The factor of 2 improvement in sensitivity in our survey relative to the Gould Belt Survey should reveal many more of these faint objects than are detected in the Gould Belt Survey.

5.2. Protoplanetary Disks

For young stars that have dispersed their envelope, a sensitivity of $\sim$2.5 mJy/beam will lead to detections of disks with $\sim$1 Earth mass of dust in Ophiuchus and 10 Earth masses in the more distant Orion region, assuming standard conversions between submillimeter emission and dust mass (e.g., Andrews et al. 2013). Large area SCUBA-2 maps of similar depth in the older σ Ori and λ Ori regions have revealed that most infrared-Class II disks have very low masses at 3–5 Myr (Williams et al. 2013; Ansdell et al. 2015), and constrain planet formation timescales more strongly than infrared surveys; similar results have been obtained from recent ALMA surveys (Ansdell et al. 2016; Barenfeld et al. 2016; Pascucci et al. 2016) and from younger regions in the Gould Belt Survey (e.g., Buckle et al. 2015; Dodds et al. 2015). Our unbiased search for disks in some of the youngest regions of nearby star formation will complement the past results from older regions to establish the evolution of the disk dust mass distribution versus evolutionary stage.

5.3. Filamentary Structure

Much of the mass in star-forming regions is located in filamentary structures (e.g., André et al. 2014). While a full understanding requires a combination of column density and velocity information, much can be learned from dust continuum observations alone. Herschel analyses (e.g., Arzoumanian et al. 2011) have suggested that filaments have a characteristic width of 0.1 pc. However, the filament width may be influenced by telescope resolution, since JCMT Gould Belt images of the Orion A molecular cloud revealed that many filaments are significantly narrower than 0.1 pc (Salji et al. 2015; Panopoulou et al. 2017). Many filaments appear to have significant substructure along both their long and short axes and may be bundles of subfilaments or fibers, which have been rarely analyzed in detail but may hold important clues to the stability and nature of the filaments (Contreras et al. 2013; Hacar et al. 2013, 2017). Deeper SCUBA-2 observations with JCMT resolution will better reveal faint extended substructure, thereby extending the range of filaments to those that are lower mass and less dense, and will allow for a robust measurement of filament widths. Extended structures on scales of $>600''$ are filtered out during data reduction to account for atmospheric changes during the observations.

The filamentary structure obtained with our deep co-added integrations will also be compared with the orientation of outflows within these regions to examine the orientation of disks in the filamentary environment. Recent results have shown axisymmetric flattened envelopes around Class 0 sources (Lee et al. 2012), while outflows are often seen perpendicular to the direction of the filament (e.g., Tobin et al. 2011). Statistics for outflows emanating from protostars that are still within their birth filamentary structures will test whether these expectations are correct, as a way to constrain the angular momentum evolution of protostars.

5.4. Nonthermal Emission from Young Stars

Young stars are magnetically active, producing X-rays and synchrotron emission with a steady and a time-variable component (Güdel 2002; Forbrich et al. 2017). Flares at millimeter and centimeter wavelengths are thought to be produced by either accretion variability or by high-energy events, which produce synchrotron emission from relativistic electrons gyrating in magnetic fields (Bower et al. 2003; Massi et al. 2006). The time-variable component appears as flares that have been seen in several sources to wavelengths as short as 3 mm (e.g., Bower et al. 2003, 2016; Salter et al. 2010; Kóspál et al. 2011), and may extend into the submillimeter due due to synchrotron self-absorption (Bower et al. 2003; Massi et al. 2006). In a few cases, correlated X-ray and infrared variability may suggest that variability of high-energy emission and accretion outbursts are not necessarily distinct phenomena (e.g., Kastner et al. 2006).

This SCUBA2 monitoring program will provide important links to longer wavelengths in the emerging context of YSO variability at infrared, X-ray, and centimeter radio wavelengths (e.g Forbrich et al. 2015, 2017). Submillimeter emission flares detected from diskless stars would be directly attributable to magnetic activity, thereby providing constraints on the electron energy distribution and the energetics of the excitation mechanism for these events. Such flares may also contaminate single-epoch submillimeter flares from protostars, though the spectral index of the 450–850 μm emission (if observed in good weather conditions) may allow us to discriminate between a nonthermal emission flare and a brief protostellar outburst.

6. Summary and Future Perspectives

Our ongoing submillimeter transient search is a novel science experiment. We are using JCMT/SCUBA-2 to monitor once per month the 450 and 850 μm emission from eight 30′ fields within nearby star-forming regions. The full survey area of 1.6 deg^2 includes 105 peaks at 850 μm brighter than 0.5 Jy/beam and 237 additional peaks brighter than 0.125–0.5 Jy/beam. Of these peaks, 93 are associated with distinct protostars or disks. In addition, 176 more protostars are fainter than 0.125 Jy/beam but increase our chances of detecting large submillimeter eruptions. The flux calibration leverages the high density of sources in each field and is now reliable to 2%–3% for bright sources, as expected for the 12 mJy/beam sensitivity of our images (Mairs et al. 2017a). This submillimeter version of differential photometry allows us to confidently quantify the stability of submillimeter sources and identify any outliers. Our survey is the first systematic, far-IR/submillimeter transient monitoring program dedicated to evaluating the variability on protostars on timescales longer than a year.

Protostellar outbursts are most often found in wide-field optical transient searches, such as the Palomar Transient Factory and ASAS-SN (e.g., Miller et al. 2011; Holoien et al. 2014). Some variability studies, such as the VVV survey and YSOVar, have targeted specific regions in the near- and mid-IR (e.g., Cody et al. 2014; Contreras Peña et al. 2017). However, these optical/near-IR searches are not sensitive to the most embedded (youngest) objects and include brightness changes related to variability in the line-of-sight extinction (e.g., Aspin 2011; Hillenbrand et al. 2013), while submillimeter luminosity should change only as the result of a variation in the protostellar luminosity.

When we began this program, we were uncertain whether any embedded young sources would show submillimeter variability. While outbursts detected at optical/near-IR wavelengths are rare (Scholz et al. 2013a; Hillenbrand & Findeisen 2015), outbursts may be much more common at younger evolutionary phases since the disks are constantly accreting from their envelopes and may need to redistribute mass to maintain stability. However, some models of protostellar evolution predict a lack of strong outbursts in the Class 0 phase (e.g., Vorobyov & Basu 2015).

Within our first year, periodic submillimeter emission has already been measured from a Class I source and will be published in a companion paper (Yoo et al. 2017); other sources show potential long-term trends. Our future efforts will establish the frequency and size of outbursts during our 3.5-year survey, and also by comparing our first year of data to the previous epoch of SCUBA-2 450 and 850 μm imaging from the JCMT Gould Belt Survey to extend time baselines to $\sim$7 years (Mairs et al. 2017b). By the end of our program, the range of variability in our sample will be able to probe the scale of disk instabilities relevant on months- and years-long timescales.

We thank the JCMT staff for their care and attention in implementing these time-sensitive observations and for help in the reduction and distribution of the data. We also thank the anonymous referee for their careful read of and comments on the manuscript.

The authors wish to recognize and acknowledge the very significant cultural role and reverence that the summit of Maunakea has always had within the indigenous Hawaiian community. We are most fortunate to have the opportunity to conduct observations from this mountain.

G.H. is supported by general grant 11473005 awarded by the National Science Foundation of China. S.M. was partially supported by the Natural Sciences and Engineering Research Council (NSERC) of Canada graduate scholarship program. D.J. is supported by the National Research Council of Canada and by an NSERC Discovery Grant. J.-E.L. was supported by the Basic Science Research Program through the National Research Foundation of Korea (NRF; grant No. NRF-2015R1A2A2A01004769) and the Korea Astronomy and Space Science Institute under the R&D program (Project No. 2015-1-320-18) supervised by the Ministry of Science, ICT and Future Planning. Partial salary support for A.P. was provided by a Canadian Institute for Theoretical Astrophysics (CITA) National Fellowship. M.K. was supported by Basic Science Research Program through the National Research Foundation of Korea(NRF) funded by the Ministry of Science, ICT & Future Planning (No. NRF-2015R1C1A1A01052160). W.K. was supported by Basic Science Research Program through the National Research Foundation of Korea (NRF) funded by the Ministry of Science, ICT & Future Planning (NRF-2016R1C1B2013642). C.-W.L. was supported by the Basic Science Research Program though the National Research Foundation of Korea (NRF) funded by the Ministry of Education, Science, and Technology (NRF-2016R1A2B4012593). E.V. acknowledges support by the Austrian Science Fund (FWF) under research grant I2549-N27. S.-P.L. is thankful for the support of the Ministry of Science and Technology (MoST) of Taiwan through Grants 102-2119-M-007-004-MY3 and 105-2119-M-007-024.

The JCMT is operated by the East Asian Observatory on behalf of The National Astronomical Observatory of Japan, Academia Sinica Institute of Astronomy and Astrophysics, the Korea Astronomy and Space Science Institute, the National Astronomical Observatories of China and the Chinese Academy of Sciences (Grant No. XDB09000000), with additional funding support from the Science and Technology Facilities Council of the United Kingdom and participating universities in the United Kingdom and Canada. The identification number for the JCMT Transient Survey under which the SCUBA-2 data used in this paper is M16AL001. The authors thank the JCMT staff for their support of the data collection and reduction efforts. The starlink software is supported by the East Asian Observatory. This research has made use of the NASA Astrophysics Data System and the facilities of the Canadian Astronomy Data Centre operated by the National Research Council of Canada with the support of the Canadian Space Agency. This research used the services of the Canadian Advanced Network for Astronomy Research (CANFAR) which in turn is supported by CANARIE, Compute Canada, University of Victoria, the National Research Council of Canada, and the Canadian Space Agency. This research made use of APLpy, an open-source plotting package for Python hosted at http://aplpy.github.com, and matplotlib, a 2D plotting library for Python (Hunter 2007).

Appendix

Table 2 lists the 850 μm peak flux per beam for bright (>125 mJy/beam) sources associated with protostars. To be associated with a protostar, the peak flux location of the emission source must be less than 7″ from the protostar position previously listed in the *Spitzer*/IRS and MIPS mid-IR photometric catalogs of Dunham et al. (2015) and Megeath et al. (2016). The emission sources are identified using the JCMT Science Archive algorithm JSA_catalog found in the Starlinks PICARD package (Gibb et al. 2013), which uses the FELLWALKER routine (for more information, see Berry 2015). The peaks are then numbered in order of brightness. Table 2 lists the 102 protostars or disks that are associated with 93 distinct bright peaks. In some cases, more than one protostar is located near a single 850 μm peak, and in one case a peak is associated with both a protostar and a disk (counted as a protostar in the numbers presented in the main text). Some associations between peaks and disks and protostars may be coincidental.

Table 2
Protostars and Disks Identified with Bright Submillimeter Peaks[a]

Region	ID	Peak[a]	Dist. (″)[b]	Name[c]	Region	ID	Peak[a]	Dist. (″)[b]	Name[c]
		Protostars					Protostars		
NGC 1333	1	9.43	0.37	J032910.4+311331	Oph Core	15	0.35	2.43	J162726.9−244050
NGC 1333	2	3.95	1.92	J032912.0+311305	Oph Core	20	0.27	5.0	J162709.4−243718
NGC 1333	2	3.95	5.92	J032912.0+311301	Oph Core	24	0.25	6.19	J162640.4−242714
NGC 1333	3	2.88	6.66	J032903.7+311603	Oph Core	25	0.25	5.89	J162623.5−242439
NGC 1333	4	2.45	2.67	J032855.5+311436	Oph Core	27	0.23	1.03	J162821.6−243623
NGC 1333	5	1.12	3.09	J032910.9+311826	Oph Core	28	0.22	5.89	J162727.9−243933
NGC 1333	5	1.12	3.39	J032911.2+311831	Oph Core	29	0.21	3.22	J162644.1−243448
NGC 1333	9	0.59	3.63	J032913.5+311358	Oph Core	32	0.19	3.84	J162705.2−243629
NGC 1333	11	0.47	2.03	J032857.3+311415	Oph Core	37	0.15	2.93	J162739.8−244315
NGC 1333	12	0.46	2.27	J032837.0+311330	Oph Core	39	0.15	5.01	J162617.2−242345
NGC 1333	13	0.44	3.07	J032904.0+311446	Serpens Main	1	6.76	3.16	J182949.6+011521
NGC 1333	17	0.37	2.1	J032900.5+311200	Serpens Main	3	2.12	1.5	J182948.1+011644
NGC 1333	21	0.32	1.45	J032917.1+312746	Serpens Main	4	1.78	2.0	J182959.2+011401
NGC 1333	21	0.32	4.25	J032917.5+312748	Serpens Main	5	1.16	6.7	J183000.7+011301
NGC 1333	22	0.32	2.56	J032907.7+312157	Serpens Main	7	1.06	2.5	J182951.1+011640
NGC 1333	24	0.27	6.63	J032840.6+311756	Serpens Main	8	0.85	1.53	J182957.7+011405
NGC 1333	28	0.23	1.78	J032834.5+310705	Serpens Main	9	0.81	4.23	J182952.2+011547
IC 348	1	1.42	2.16	J034356.5+320052	Serpens Main	15	0.28	2.54	J182931.9+011842
IC 348	2	1.16	2.68	J034356.8+320304	Serpens South	10	0.66	5.56	J182938.1−015100
IC 348	3	0.57	2.64	J034443.9+320136	Serpens South	17	0.45	3.0	J183025.8−021042
IC 348	3	0.57	6.51	J034443.3+320131	Serpens South	25	0.3	6.7	J182959.4−020106
IC 348	4	0.34	1.27	J034350.9+320324	Serpens South	31	0.2	4.0	J183001.0−020608
IC 348	9	0.15	1.14	J034412.9+320135	Serpens South	32	0.2	5.74	J183017.4−020958
OMC 2/3	2	5.96	6.53	2293	Serpens South	32	0.2	5.91	J183017.0−020958
OMC 2/3	3	5.6	3.08	2433	Serpens South	34	0.2	6.46	J183015.6−020719
OMC 2/3	6	2.66	5.8	2302	Serpens South	40	0.16	6.0	J182947.0−015548
OMC 2/3	7	2.54	3.24	2437	Serpens South	42	0.16	3.98	J182912.8−020350
OMC 2/3	13	1.74	3.53	2369	Serpens South	43	0.16	2.62	J182943.9−021255
OMC 2/3	13	1.74	6.85	2366	Serpens South	45	0.15	1.66	J182943.3−015651
OMC 2/3	17	1.58	3.51	2407					
OMC 2/3	18	1.46	1.94	2323			Disks		
OMC 2/3	20	1.39	1.25	2254	NGC 1333	32	0.16	5.88	J032856.1+311908
OMC 2/3	21	1.34	4.93	2469	OMC 2/3	5	3.62	2.94	2072
OMC 2/3	22	1.25	3.91	2187	OMC 2/3	15	1.63	6.6	2334
OMC 2/3	76	0.26	5.2	2456	OMC 2/3	19	1.45	3.98	2029
OMC 2/3	86	0.22	2.6	2510	OMC 2/3	25	1.06	4.84	2345
NGC 2068	1	2.54	3.79	3166	OMC 2/3	29	0.78	6.67	2371
NGC 2068	5	1.02	5.12	3201	OMC 2/3	47	0.45	1.07	2179
NGC 2068	5	1.02	5.78	3202	OMC 2/3	51	0.41	1.99	2347
NGC 2068	6	0.62	5.72	3168	OMC 2/3	61	0.32	3.8	2184
NGC 2068	6	0.62	5.76	3167	OMC 2/3	72	0.28	6.81	2145
NGC 2068	7	0.59	4.92	3203	OMC 2/3	75	0.26	5.35	2333
NGC 2068	8	0.57	2.94	3211	OMC 2/3	83	0.23	4.72	2363
NGC 2068	11	0.52	2.25	3159	OMC 2/3	101	0.19	6.31	2228
NGC 2068	13	0.44	6.25	3215	NGC 2024	30	0.17	3.33	2927
NGC 2068	22	0.29	0.83	3160	Oph Core	4	0.66	6.25	J162624.0−241613
NGC 2068	24	0.29	1.16	3180	Oph Core	6	0.59	4.36	J162645.0−242307
NGC 2024	4	5.94	3.37	2955	Oph Core	8	0.47	6.24	J162323.6−244314
NGC 2024	6	0.82	6.71	2867	Oph Core	18	0.28	4.89	J162610.3−242054
NGC 2024	26	0.19	4.02	3085	Oph Core	36	0.17	2.96	J162816.5−243657
Oph Core	2	3.98	5.3	J162626.4−242430	Oph Core	40	0.14	2.99	J162715.8−243843
Oph Core	13	0.39	3.71	J162730.1−242743	Serpens South	31	0.2	5.41	J183001.3−020609

Notes.
[a] Jy beam^{-1}.
[b] Distance between centroid of submillimeter peak and mid-IR position.
[c] Dunham et al. (2015) and Megeath et al. (2016).

ORCID iDs

Gregory J. Herczeg https://orcid.org/0000-0002-7154-6065
Doug Johnstone https://orcid.org/0000-0002-6773-459X
Steve Mairs https://orcid.org/0000-0002-6956-0730
Jennifer Hatchell https://orcid.org/0000-0002-4870-2760
Jeong-Eun Lee https://orcid.org/0000-0003-3119-2087
Geoffrey C. Bower https://orcid.org/0000-0003-4056-9982
Huei-Ru Vivien Chen https://orcid.org/0000-0002-9774-1846
Yuri Aikawa https://orcid.org/0000-0003-3283-6884
Sung-Ju Kang https://orcid.org/0000-0002-5004-7216
Miju Kang https://orcid.org/0000-0002-5016-050X
Wen-Ping Chen https://orcid.org/0000-0003-0262-272X
Jonathan P. Williams https://orcid.org/0000-0001-5058-695X
Jaehan Bae https://orcid.org/0000-0001-7258-770X
Michael M. Dunham https://orcid.org/0000-0003-0749-9505
Eduard I. Vorobyov https://orcid.org/0000-0002-6045-0359
Zhaohuan Zhu https://orcid.org/0000-0003-3616-6822
Ramprasad Rao https://orcid.org/0000-0002-1407-7944
Helen Kirk https://orcid.org/0000-0002-5779-8549
Kevin Lacaille https://orcid.org/0000-0001-9870-5663
James Lane https://orcid.org/0000-0001-8472-6404
Andy Pon https://orcid.org/0000-0003-4612-1812
Aleks Scholz https://orcid.org/0000-0001-8993-5053
Graham S. Bell https://orcid.org/0000-0003-0438-8228
Sarah Graves https://orcid.org/0000-0001-9361-5781
Harriet Parsons https://orcid.org/0000-0002-6327-3423
Mi-Ryang Kim https://orcid.org/0000-0002-1408-7747
Eun Jung Chung https://orcid.org/0000-0003-0014-1527
Stewart P. S. Eyres https://orcid.org/0000-0002-6663-7675
Jan Forbrich https://orcid.org/0000-0001-8694-4966
Shu-ichiro Inutsuka https://orcid.org/0000-0003-4366-6518
Kyoung Hee Kim https://orcid.org/0000-0001-9597-7196
Woojin Kwon https://orcid.org/0000-0003-4022-4132
Shih-Ping Lai https://orcid.org/0000-0001-5522-486X
Chang Won Lee https://orcid.org/0000-0002-3179-6334
Chin-Fei Lee https://orcid.org/0000-0002-3024-5864
Feng Long https://orcid.org/0000-0002-7607-719X
A-Ran Lyo https://orcid.org/0000-0002-9907-8427
Lei Qian https://orcid.org/0000-0003-0597-0957
Dimitris Stamatellos https://orcid.org/0000-0002-4502-8344
Shigehisa Takakuwa https://orcid.org/0000-0003-0845-128X
Ya-Wen Tang https://orcid.org/0000-0002-0675-276X

References

Allen, L. E., Myers, P. C., Di Francesco, J., et al. 2002, ApJ, 566, 993
André, P., Di Francesco, J., Ward-Thompson, D., et al. 2014, in Protostars and Planets VI, ed. H. Beuther et al. (Tucson, AZ: Univ. Arizona Press), 27
André, P., Ward-Thompson, D., & Barsony, M. 1993, ApJ, 406, 122
Andrews, S. M., Rosenfeld, K. A., Kraus, A. L., & Wilner, D. J. 2013, ApJ, 771, 129
Ansdell, M., Williams, J. P., & Cieza, L. A. 2015, ApJ, 806, 221
Ansdell, M., Williams, J. P., van der Marel, N., et al. 2016, arXiv:1604.05719
Armitage, P. J. 2015, arXiv:1509.06382
Armitage, P. J. 2016, ApJL, 833, L15
Armitage, P. J., Livio, M., & Pringle, J. E. 2001, MNRAS, 324, 705
Arzoumanian, D., André, P., Didelon, P., et al. 2011, A&A, 529, L6
Aso, Y., Tatematsu, K., Sekimoto, Y., et al. 2000, ApJS, 131, 465
Aspin, C. 2011, AJ, 142, 135
Aspin, C., Reipurth, B., Herczeg, G. J., & Capak, P. 2010, ApJL, 719, L50
Audard, M., Ábrahám, P., Dunham, M. M., et al. 2014, in Protostars and Planets VI, ed. H. Beuther et al. (Tucson, AZ: Univ. Arizona Press), 387
Bae, J., Hartmann, L., Zhu, Z., & Nelson, R. P. 2014, ApJ, 795, 61
Bae, J., Nelson, R. P., Hartmann, L., & Richard, S. 2016, ApJ, 829, 13
Bally, J., Devine, D., & Reipurth, B. 1996, ApJL, 473, L49
Bally, J., Lanber, W. D., Stark, A. A., & Wilson, R. W. 1987, ApJL, 312, L45
Bally, J., Walawender, J., Johnstone, D., Kirk, H., & Goodman, A. 2008, in Handbook of Star Forming Regions, Vol. 1, The Northern Sky, ed. B. Reipurth (San Francisco, CA: ASP), 308
Balog, Z., Muzerolle, J., Flaherty, K., et al. 2014, ApJL, 789, L38
Baraffe, I., & Chabrier, G. 2010, A&A, 521, A44
Baraffe, I., Elbakyan, V. G., Vorobyov, E. I., & Chabrier, G. 2017, A&A, 597, A19
Barenfeld, S. A., Carpenter, J. M., Ricci, L., & Isella, A. 2016, arXiv:1605.05772
Bell, K. R., Lin, D. N. C., Hartmann, L. W., & Kenyon, S. J. 1995, ApJ, 444, 376
Berry, D. S. 2015, A&C, 10, 22
Billot, N., Morales-Calderón, M., Stauffer, J. R., Megeath, S. T., & Whitney, B. 2012, ApJL, 753, L35
Bonnell, I., & Bastien, P. 1992, ApJL, 401, L31
Bontemps, S., Andre, P., & Ward-Thompson, D. 1995, A&A, 297, 98
Bourke, T. L., Myers, P. C., Evans, N. J., II, et al. 2006, ApJL, 649, L37
Bower, G. C., Loinard, L., Dzib, S., et al. 2016, ApJ, 830, 107
Bower, G. C., Plambeck, R. L., Bolatto, A., et al. 2003, ApJ, 598, 1140
Buckle, J. V., Drabek-Maunder, E., Greaves, J., et al. 2015, MNRAS, 449, 2472
Caratti o Garatti, A., Garcia Lopez, R., Scholz, A., et al. 2011, A&A, 526, L1
Caratti O Garatti, A., Stecklum, B., Garcia Lopez, R., et al. 2016, NatPh, 13, 276
Casali, M. M., Eiroa, C., & Duncan, W. D. 1993, A&A, 275, 195
Chen, M. C.-Y., Di Francesco, J., Johnstone, D., et al. 2016, ApJ, 826, 95
Chini, R., Reipurth, B., Ward-Thompson, D., et al. 1997, ApJL, 474, L135
Choi, M., Kang, M., Byun, D.-Y., & Lee, J.-E. 2012, ApJ, 759, 136
Cieza, L., Williams, J., Kourkchi, E., et al. 2015, MNRAS, 454, 1909
Cieza, L. A., Casassus, S., Tobin, J., et al. 2016, arXiv:1607.03757
Cody, A. M., Hillenbrand, L. A., David, T. J., et al. 2017, ApJ, 836, 41
Cody, A. M., Stauffer, J., Baglin, A., et al. 2014, AJ, 147, 82
Contreras Peña, C., Lucas, P. W., Minniti, D., et al. 2017, MNRAS, 465, 3011
Contreras, Y., Rathborne, J., & Garay, G. 2013, MNRAS, 433, 251
Costigan, G., Vink, J. S., Scholz, A., Ray, T., & Testi, L. 2014, MNRAS, 440, 3444
Curtis, E. I., Richer, J. S., Swift, J. J., & Williams, J. P. 2010, MNRAS, 408, 1516
D'Angelo, C. R., & Spruit, H. C. 2010, MNRAS, 406, 1208
Davis, C. J., Matthews, H. E., Ray, T. P., Dent, W. R. F., & Richer, J. S. 1999, MNRAS, 309, 141
Dempsey, J. T., Friberg, P., Jenness, T., et al. 2013, MNRAS, 430, 2534
Dodds, P., Greaves, J. S., Scholz, A., et al. 2015, MNRAS, 447, 722
Duarte-Cabral, A., Fuller, G. A., Peretto, N., et al. 2010, A&A, 519, A27
Dunham, M. M., Allen, L. E., Evans, N. J., II, et al. 2015, ApJS, 220, 11
Dunham, M. M., Crapsi, A., Evans, N. J., II, et al. 2008, ApJS, 179, 249
Dunham, M. M., Evans, N. J., II, Terebey, S., Dullemond, C. P., & Young, C. H. 2010, ApJ, 710, 470
Dunham, M. M., Stutz, A. M., Allen, L. E., et al. 2014, in Protostars and Planets VI, ed. H. Beuther et al. (Tucson, AZ: Univ. Arizona Press), 195
Dunham, M. M., & Vorobyov, E. I. 2012, ApJ, 747, 52
Eiroa, C., Djupvik, A. A., & Casali, M. M. 2008, in Handbook of Star Forming Regions, Vol. 2, The Southern Sky, ed. B. Reipurth (San Francisco, CA: ASP), 693
Elbakyan, V. G., Vorobyov, E. I., & Glebova, G. M. 2016, ARep, 60, 879
Elias, J. H. 1978, ApJ, 224, 453
Enoch, M. L., Evans, N. J., II, Sargent, A. I., & Glenn, J. 2009, ApJ, 692, 973
Enoch, M. L., Glenn, J., Evans, N. J., II, et al. 2007, ApJ, 666, 982
Enoch, M. L., Young, K. E., Glenn, J., et al. 2006, ApJ, 638, 293
Fischer, W. J., Megeath, S. T., Furlan, E., et al. 2017, ApJ, 840, 69
Fischer, W. J., Megeath, S. T., Tobin, J. J., et al. 2012, ApJ, 756, 99
Forbrich, J., Reid, M. J., Menten, K. M., et al. 2017, arXiv:1706.05562
Forbrich, J., Rodríguez, L. F., Palau, A., et al. 2015, ApJ, 814, 15
Forgan, D., & Rice, K. 2010, MNRAS, 402, 1349
Friesen, R. K., Bourke, T. L., Di Francesco, J., Gutermuth, R., & Myers, P. C. 2016, ApJ, 833, 204
Friesen, R. K., Di Francesco, J., Shirley, Y. L., & Myers, P. C. 2009, ApJ, 697, 1457
Frimann, S., Jørgensen, J. K., Dunham, M. M., et al. 2017, arXiv:1703.10225

Gaia Collaboration, Brown, A. G. A., Vallenari, A., et al. 2016, arXiv:1609.04172
Gibb, A. G. 2008, in Handbook of Star Forming Regions, Vol. 1, The Northern Sky, ed. B. Reipurth (San Francisco, CA: ASP), 693
Gibb, A. G., Jenness, T., & Economou, F. 2013, StaUN, 265
Graves, S. F., Richer, J. S., Buckle, J. V., et al. 2010, MNRAS, 409, 1412
Green, J. D., Evans, N. J., II, Kóspál, Á, et al. 2013, ApJ, 772, 117
Green, J. D., Kraus, A. L., Rizzuto, A. C., et al. 2016, ApJ, 830, 29
Güdel, M. 2002, ARA&A, 40, 217
Gutermuth, R. A., Bourke, T. L., Allen, L. E., et al. 2008b, ApJL, 673, L151
Gutermuth, R. A., Myers, P. C., Megeath, S. T., et al. 2008a, ApJ, 674, 336
Hacar, A., Tafalla, M., & Alves, J. 2017, arXiv:1703.07029
Hacar, A., Tafalla, M., Kauffmann, J., & Kovács, A. 2013, A&A, 554, A55
Harsono, D., Bruderer, S., & van Dishoeck, E. F. 2015, A&A, 582, A41
Hartmann, L., Cassen, P., & Kenyon, S. J. 1997, ApJ, 475, 770
Hartmann, L., Herczeg, G., & Calvet, N. 2016, ARA&A, 54, 135
Hartmann, L., & Kenyon, S. J. 1985, ApJ, 299, 462
Hartmann, L., & Kenyon, S. J. 1996, ARA&A, 34, 207
Harvey, P., Merín, B., Huard, T. L., et al. 2007, ApJ, 663, 1149
Hatchell, J., Richer, J. S., Fuller, G. A., et al. 2005, A&A, 440, 151
Hatchell, J., Wilson, T., Drabek, E., et al. 2013, MNRAS, 429, L10
Haubois, X., Dodds-Eden, K., Weiss, A., et al. 2012, A&A, 540, A41
Hennebelle, P., Lesur, G., & Fromang, S. 2017, A&A, 599, A86
Herbig, G. H. 1977, ApJ, 217, 693
Herbig, G. H. 2008, AJ, 135, 637
Herbst, W. 2008, in Handbook of Star Forming Regions, Vol. 1, The Northern Sky, ed. B. Reipurth (San Francisco, CA: ASP), 372
Hillenbrand, L. A., & Findeisen, K. P. 2015, ApJ, 808, 68
Hillenbrand, L. A., Miller, A. A., Covey, K. R., et al. 2013, AJ, 145, 59
Hodapp, K. W. 1999, AJ, 118, 1338
Hodapp, K. W., & Chini, R. 2015, ApJ, 813, 107
Hodapp, K. W., Chini, R., Watermann, R., & Lemke, R. 2012, ApJ, 744, 56
Holland, W. S., Bintley, D., Chapin, E. L., et al. 2013, MNRAS, 430, 2513
Holoien, T. W.-S., Prieto, J. L., Stanek, K. Z., et al. 2014, ApJL, 785, L35
Hsieh, T.-H., Lai, S.-P., Belloche, A., & Wyrowski, F. 2016, arXiv:1605.03055
Hsieh, T.-H., Lai, S.-P., Belloche, A., Wyrowski, F., & Hung, C.-L. 2015, ApJ, 802, 126
Hunter, J. D. 2007, CSE, 9, 90
Hunter, T. R., Brogan, C. L., MacLeod, G., et al. 2017, arXiv:1701.08637
Johnstone, D., & Bally, J. 1999, ApJL, 510, L49
Johnstone, D., Di Francesco, J., & Kirk, H. 2004, ApJL, 611, L45
Johnstone, D., Hendricks, B., Herczeg, G. J., & Bruderer, S. 2013, ApJ, 765, 133
Johnstone, D., Matthews, H., & Mitchell, G. F. 2006, ApJ, 639, 259
Johnstone, D., Wilson, C. D., Moriarty-Schieven, G., et al. 2000, ApJ, 545, 327
Jørgensen, J. K., Johnstone, D., Kirk, H., et al. 2008, ApJ, 683, 822
Jørgensen, J. K., Johnstone, D., Kirk, H., & Myers, P. C. 2007, ApJ, 656, 293
Jørgensen, J. K., Visser, R., Sakai, N., et al. 2013, ApJL, 779, L22
Jørgensen, J. K., Visser, R., Williams, J. P., & Bergin, E. A. 2015, A&A, 579, A23
Kaas, A. A., Olofsson, G., Bontemps, S., et al. 2004, A&A, 421, 623
Kackley, R., Scott, D., Chapin, E., & Friberg, P. 2010, Proc. SPIE, 7740, 77401Z
Kamazaki, T., Saito, M., Hirano, N., & Kawabe, R. 2001, ApJ, 548, 278
Kastner, J. H., Richmond, M., Grosso, N., et al. 2006, ApJL, 648, L43
Kenyon, S. J., Hartmann, L. W., Strom, K. M., & Strom, S. E. 1990, AJ, 99, 869
Kern, N. S., Keown, J. A., Tobin, J. J., Mead, A., & Gutermuth, R. A. 2016, AJ, 151, 42
Kim, H. J., Evans, N. J., II, Dunham, M. M., Lee, J.-E., & Pontoppidan, K. M. 2012, ApJ, 758, 38
Kirk, H., Johnstone, D., & Di Francesco, J. 2006, ApJ, 646, 1009
Kirk, H., Johnstone, D., Di Francesco, J., et al. 2016, ApJ, 821, 98
Kirk, H., Myers, P. C., Bourke, T. L., et al. 2013, ApJ, 766, 115
Knee, L. B. G., & Sandell, G. 2000, A&A, 361, 671
Kóspál, Á, Ábrahám, P., Csengeri, T., et al. 2017, ApJ, 843, 45
Kóspál, Á, Ábrahám, P., Prusti, T., et al. 2007, A&A, 470, 211
Kóspál, Á, Salter, D. M., Hogerheijde, M. R., Moór, A., & Blake, G. A. 2011, A&A, 527, A96
Kounkel, M., Hartmann, L., Loinard, L., et al. 2017, ApJ, 834, 142
Kutner, M. L., Tucker, K. D., Chin, G., & Thaddeus, P. 1977, ApJ, 215, 521
Lada, E. A., Evans, N. J., II, & Falgarone, E. 1997, ApJ, 488, 286
Lane, J., Kirk, H., Johnstone, D., et al. 2016, ApJ, 833, 44
Larson, R. B. 1969, MNRAS, 145, 271
Lee, C. W., Bourke, T. L., Myers, P. C., et al. 2009, ApJ, 693, 1290
Lee, C. W., Kim, M.-R., Kim, G., et al. 2013, ApJ, 777, 50
Lee, K., Looney, L., Johnstone, D., & Tobin, J. 2012, ApJ, 761, 171
Lee, K. I., Fernández-López, M., Storm, S., et al. 2014, ApJ, 797, 76
Lin, D. N. C., Faulkner, J., & Papaloizou, J. 1985, MNRAS, 212, 105
Loinard, L., Torres, R. M., Mioduszewski, A. J., & Rodríguez, L. F. 2008, ApJL, 675, L29
Loren, R. B., & Wootten, A. 1986, ApJ, 306, 142
Loren, R. B., Wootten, A., & Wilking, B. A. 1990, ApJ, 365, 269
Luhman, K. L., Esplin, T. L., & Loutrel, N. P. 2016, ApJ, 827, 52
Machida, M. N., Inutsuka, S.-i., & Matsumoto, T. 2011, ApJ, 729, 42
Mairs, S., Johnstone, D., Kirk, H., et al. 2015, MNRAS, 454, 2557
Mairs, S., Johnstone, D., Kirk, H., et al. 2017b, ApJ, in press (arXiv:1710.03761)
Mairs, S., Lane, J., Johnstone, D., et al. 2017a, arXiv:1706.01897
Massi, M., Forbrich, J., Menten, K. M., et al. 2006, A&A, 453, 959
Masunaga, H., & Inutsuka, S.-I. 2000, ApJ, 531, 350
Maury, A. J., André, P., Men'shchikov, A., Könyves, V., & Bontemps, S. 2011, A&A, 535, A77
Megeath, S. T., Gutermuth, R., Muzerolle, J., et al. 2012, AJ, 144, 192
Megeath, S. T., Gutermuth, R., Muzerolle, J., et al. 2016, AJ, 151, 5
Meyer, M. R., Flaherty, K., Levine, J. L., et al. 2008, in Handbook of Star Forming Regions, Vol. 1, The Northern Sky, ed. B. Reipurth (San Francisco, CA: ASP), 662
Mezger, P. G., Zylka, R., & Wink, J. E. 1990, A&A, 228, 95
Miller, A. A., Hillenbrand, L. A., Covey, K. R., et al. 2011, ApJ, 730, 80
Motte, F., André, P., & Neri, R. 1998, A&A, 336, 150
Muñoz, D. J., & Lai, D. 2016, ApJ, 827, 43
Muzerolle, J., Furlan, E., Flaherty, K., Balog, Z., & Gutermuth, R. 2013, Natur, 493, 378
Myers, P. C. 2012, ApJ, 752, 9
Nakamura, F., Takakuwa, S., & Kawabe, R. 2012, ApJL, 758, L25
Nutter, D., & Ward-Thompson, D. 2007, MNRAS, 374, 1413
Offner, S. S. R., & McKee, C. F. 2011, ApJ, 736, 53
Olmi, L., & Testi, L. 2002, A&A, 392, 1053
Onozato, H., Ita, Y., Ono, K., et al. 2015, PASJ, 67, 39
Ortiz-León, G. N., Dzib, S. A., Kounkel, M. A., et al. 2017a, ApJ, 834, 143
Ortiz-León, G. N., Loinard, L., Kounkel, M. A., et al. 2017b, ApJ, 834, 141
Owen, J. E., & Jacquet, E. 2015, MNRAS, 446, 3285
Pan, Z., Li, D., Chang, Q., et al. 2017, ApJ, 836, 194
Panopoulou, G. V., Psaradaki, I., Skalidis, R., Tassis, K., & Andrews, J. J. 2017, MNRAS, 466, 2529
Pascucci, I., Testi, L., Herczeg, G. J., et al. 2016, arXiv:1608.03621
Pattle, K., Ward-Thompson, D., Kirk, J. M., et al. 2015, MNRAS, 450, 1094
Pattle, K., Ward-Thompson, D., Kirk, J. M., et al. 2017, MNRAS, 464, 4255
Peterson, D. E., Megeath, S. T., Luhman, K. L., et al. 2008, ApJ, 685, 313
Plunkett, A. L., Arce, H. G., Mardones, D., et al. 2015, Natur, 527, 70
Pon, A., Plume, R., Friesen, R. K., et al. 2009, ApJ, 698, 1914
Raga, A. C., de Gouveia Dal Pino, E. M., Noriega-Crespo, A., Mininni, P. D., & Velázquez, P. F. 2002, A&A, 392, 267
Rebull, L. M., Cody, A. M., Covey, K. R., et al. 2014, AJ, 148, 92
Reipurth, B. 1989, Natur, 340, 42
Reipurth, B., & Aspin, C. 2004, ApJL, 606, L119
Romanova, M. M., Ustyugova, G. V., Koldoba, A. V., & Lovelace, R. V. E. 2013, MNRAS, 430, 699
Sadavoy, S. I., Di Francesco, J., Bontemps, S., et al. 2010, ApJ, 710, 1247
Safron, E. J., Fischer, W. J., Megeath, S. T., et al. 2015, ApJL, 800, L5
Salji, C. J., Richer, J. S., Buckle, J. V., et al. 2015, MNRAS, 449, 1782
Salter, D. M., Kóspál, Á, Getman, K. V., et al. 2010, A&A, 521, A32
Scholz, A., Froebrich, D., & Wood, K. 2013a, MNRAS, 430, 2910
Scholz, A., Geers, V., Clark, P., Jayawardhana, R., & Muzic, K. 2013b, ApJ, 775, 138
Scholz, A., Jayawardhana, R., Muzic, K., et al. 2012a, ApJ, 756, 24
Scholz, A., Muzic, K., Geers, V., et al. 2012b, ApJ, 744, 6
Shu, F. H. 1977, ApJ, 214, 488
Shu, F. H., Adams, F. C., & Lizano, S. 1987, ARA&A, 25, 23
Skinner, S., Gagné, M., & Belzer, E. 2003, ApJ, 598, 375
Spezzi, L., Petr-Gotzens, M. G., Alcalá, J. M., et al. 2015, A&A, 581, A140
Stamatellos, D., Whitworth, A. P., & Hubber, D. A. 2011, ApJ, 730, 32
Stamatellos, D., Whitworth, A. P., & Hubber, D. A. 2012, MNRAS, 427, 1182
Stanke, T., Smith, M. D., Gredel, R., & Khanzadyan, T. 2006, A&A, 447, 609
Strom, S. E., Vrba, F. J., & Strom, K. M. 1976, AJ, 81, 638
Stutz, A. M., Tobin, J. J., Stanke, T., et al. 2013, ApJ, 767, 36
Takahashi, S., Ho, P. T. P., Teixeira, P. S., Zapata, L. A., & Su, Y.-N. 2013, ApJ, 763, 57
Takahashi, S., Saigo, K., Ho, P. T. P., & Tomida, K. 2012, ApJ, 752, 10
Takahashi, S., Saito, M., Ohashi, N., et al. 2008, ApJ, 688, 344

Tetarenko, A. J., Sivakoff, G. R., Miller-Jones, J. C. A., et al. 2017, MNRAS, 469, 3141
Thronson, H. A., Jr., Lada, C. J., Schwartz, P. R., et al. 1984, ApJ, 280, 154
Tobin, J. J., Hartmann, L., Chiang, H.-F., et al. 2011, ApJ, 740, 45
Tobin, J. J., Stutz, A. M., Megeath, S. T., et al. 2015, ApJ, 798, 128
Tsujimoto, M., Koyama, K., Tsuboi, Y., Goto, M., & Kobayashi, N. 2002, ApJ, 566, 974
van Leeuwen, F. 2007, A&A, 474, 653
Venuti, L., Bouvier, J., Flaccomio, E., et al. 2014, A&A, 570, A82
Visser, A. E., Richer, J. S., Chandler, C. J., & Padman, R. 1998, MNRAS, 301, 585
Visser, R., Bergin, E. A., & Jørgensen, J. K. 2015, A&A, 577, A102
Vorobyov, E., Elbakyan, V., Hosokawa, T., et al. 2017a, arXiv:1706.00502
Vorobyov, E. I., Baraffe, I., Harries, T., & Chabrier, G. 2013, A&A, 557, A35
Vorobyov, E. I., & Basu, S. 2005, ApJL, 633, L137
Vorobyov, E. I., & Basu, S. 2010, ApJ, 719, 1896
Vorobyov, E. I., & Basu, S. 2015, ApJ, 805, 115
Vorobyov, E. I., Elbakyan, V., Dunham, M. M., & Guedel, M. 2017b, A&A, 600, A36
Vorobyov, E. I., Pavlyuchenkov, Y. N., & Trinkl, P. 2014, ARep, 58, 522
Vrba, F. J. 1977, AJ, 82, 198
Walawender, J., Bally, J., Francesco, J. D., Jørgensen, J., & Getman, K. 2008, in Handbook of Star Forming Regions, Vol. 1, The Northern Sky, ed. B. Reipurth (San Francisco, CA: ASP), 346
Walawender, J., Bally, J., Kirk, H., et al. 2006, AJ, 132, 467
Ward-Thompson, D., Di Francesco, J., Hatchell, J., et al. 2007, PASP, 119, 855
White, G. J., Drabek-Maunder, E., Rosolowsky, E., et al. 2015, MNRAS, 447, 1996
Wilking, B. A., Gagné, M., & Allen, L. E. 2008, in Handbook of Star Forming Regions, Vol. 2, The Southern Sky, ed. B. Reipurth (San Francisco, CA: ASP), 351
Williams, J. P., Cieza, L. A., Andrews, S. M., et al. 2013, MNRAS, 435, 1671
Williams, J. P., Plambeck, R. L., & Heyer, M. H. 2003, ApJ, 591, 1025
Yan, J., Wang, H., Wang, M., et al. 1998, AJ, 116, 2438
Young, C. H., Jørgensen, J. K., Shirley, Y. L., et al. 2004, ApJS, 154, 396
Young, K. E., Enoch, M. L., Evans, N. J., II, et al. 2006, ApJ, 644, 326
Yoo, H., Lee, J.-E., Mairs, S., et al. 2017, ApJ, in press (arXiv:1709.04096)
Zhu, Z., Hartmann, L., Calvet, N., et al. 2008, ApJ, 684, 1281
Zhu, Z., Hartmann, L., Gammie, C., & McKinney, J. C. 2009, ApJ, 701, 620
Zhu, Z., Hartmann, L., Gammie, C. F., et al. 2010, ApJ, 713, 1134